Progress of Theoretical Physics, Vol. 123, No. 2, February 2010

Averaged Semiquantum Method Is a Useful Tool to Predict the Decoherence of Kicked Harmonic Oscillator System

Zhuo WANG*) and Quan-lin JIE

Department of Physics, Wuhan University, Wuhan 430072, P. R. China

(Received September 23, 2009; Revised November 17, 2009)

We investigate the quantum-classical correspondence of kicked harmonic oscillator (KHO) model by the averaged semiquantum method. Furthermore, we investigate the decoherence of N dimensional kicked harmonic oscillator with different coupling strengths and the dimensionalities. The averaged semiquantum method origins from the time-dependent variational principle (TDVP) formulation and contains nondiagonal matrix elements, so it can be applied to study dissipation, measurement and decoherence problems. When applied to the harmonic oscillator model coupled to a heat bath with different coupling strengths and dimensionalities of the bath, we find that the loss of coherence between superposed wave packets can be also predicted by the averaged semiquantum method.

Subject Index: 020, 024, 046, 061, 062

§1. Introduction

Semiquantum method has a wide application in many branches of physics. Recent years, this method has been used to study the nonlinear dynamics and chaos.[1)] It is also named as squeezed state dynamics[2)] or Gaussian wave-packet dynamics,[3)] and origins from the time-dependent variational principle (TDVP) formulation, $\Gamma = \int dt \, \langle \Psi(t)| i\hbar \frac{\partial}{\partial t} - \hat{H} \, |\Psi(t)\rangle$ with $\delta\Gamma = 0$. This approach enables us to study the effects of the quantum fluctuations on dynamical behavior.[4),5)] Moreover, it has been proven to be successful in the investigation of dynamical systems ranging from integrable to many-body nonintegrable systems,[6)] which is usually associated with reduced density matrix evolving in time according to the Liouville von-Neumann equation. The method simplifies the quantum version and gives better results than the semiclassical approach.

The semiquantum dynamics of one-dimensional kicked harmonic oscillator has been extensively investigated. Three different energy diffusions have been observed, namely localization, linear diffusion, and quadratic diffusion.[2)] We consider the semiquantum method to investigate decoherence which is usually handled by master equation. The master equation is derived under specific assumptions for high dimensional system under supposition of certain temperature.[7)] For large coupling constants and long time scales, it can be accomplished in a formally exact manner by path integrals for open quantum systems.[7)] Furthermore, Monte Carlo wavefunction techniques[8)−14)] are extensively used to treat master equations in the weak coupling or Markovian limit. Recently, stochastic equation[15)−18)] is used to treat the system-environment problem, which can describe the long-time evolution exactly.

*) E-mail: wangzhuoxxh@yahoo.com.cn

One-dimensional KHO was originally proposed as a two-dimensional model of kicked charges in a uniform magnetic.[8] The classical and quantum dynamics properties of one-dimensional KHO, which does not obey the Kolmogorov-Arnold-Moser (KAM) theorem,[9),10)] have attracted much attention.[11),12)] Environmental effect on kicked system was first studied by Dittrich and Graham.[23)] We consider the KHO system with various external degrees of freedom. The dynamics of the coupled system is governed by the Hamiltonian

$$\begin{aligned} H &= H_{\text{system}} + H_{\text{bath}} + H_{\text{coupling}}, \\ H_{\text{system}} &= \frac{p^2}{2m} + \frac{1}{2}m\omega_0^2 q^2 - K\cos(q)\sum_{n=0}^{\infty}\delta(t-n\tau), \\ H_{\text{bath}} &= \sum_{i=1}^{N}\left(\frac{p_i^2}{2m} + \frac{1}{2}m\omega_i^2 q_i^2 - K\cos(q_i)\sum_{n=0}^{\infty}\delta(t-n\tau)\right), \\ H_{\text{coupling}} &= q\sum_{i=1}^{N}\lambda_i q_i. \end{aligned} \tag{1}$$

Here ω_i is the oscillator frequency, K is the amplitude of the kick, τ is the interval between two consecutive kicks, and λ_i is the coupling strength.

The aim of this paper is to introduce the averaged semiquantum method and use it to predict decoherence. In §2, we describe the averaged semiquantum method. In §3, we use the averaged semiquantum method to study the quantum-classical transition in low dimensional KHO system, and show the agreement of decoherence function and linear entropy. In §4, we illustrate numerically the decoherence of a superposition of two symmetrically located coherent states and compare with the master equation results. In §5, we calculate the decoherence function for high dimensional case with different coupling strength. Finally, we draw conclusions.

§2. Averaged semiquantum method

In this section, we obtain an equation of motion for the reduced system dynamics, and the environment effect is incorporated through a mean field. We consider here an $\boldsymbol{N}$ coupled model described by a Hamiltonian

$$H = h_S + h_E + h_I, \tag{2}$$

where h_S is the Hamiltonian for the system, which consists of a few degrees of freedom, h_E the Hamiltonian for the environment, and h_I the coupling. Here we assume that the interaction is written

$$h_I = Q \otimes B, \tag{3}$$

where $Q \equiv \{q_i^s\}_{i=1,\cdots,n_s} B \equiv \{q_i\}_{i=1,\cdots,n_B}$ correspond to functions of two sets of operators of the system and environment, respectively.

Averaged semiquantum method to the study of time-dependent quantum dynamics origins from the result of the variational principle

$$\langle\delta\psi|\, i\hbar\partial_t - H_I\,|\psi\rangle = 0. \tag{4}$$

The wave function is represented as

$$|\psi\rangle = |\psi_0\rangle \prod_{k=1}^{N} |\psi_k\rangle, \tag{5}$$

where $|\psi_k\rangle$ is the single-particle wave function for kth degree of freedom of the environment and N is the total number of degrees of freedom. $|\psi_0\rangle$ is the wave function for the system.

Furthermore, we choose the Gaussian wave packet, which is widely used in the semiquantum method, to describe.

$$|\psi_k^{\rangle} = (2\pi\hbar\bar{G}_k)^{-1/4} \exp\left[-\frac{1}{2\hbar}(q-\bar{q}_k)^2\left(\frac{1}{2}\bar{G}_k^{-1} - 2i\bar{\prod}_k\right) + i\bar{p}_k(q-\bar{q}_k)/\hbar\right], \tag{6}$$

where $\bar{G}_k$, $\bar{\prod}_k$, $\bar{q}_k$ and $\bar{p}_k$ are all time-dependent.

The initial conditions of the bath can be sampled from the Wigner distribution at the saddle points, or from the classical action-angle variables

$$\begin{aligned} G_k(0) &= 1/2a_k\hbar, \\ \Pi_k(0) &= 0, \\ q_k^{\text{inital}}(0) &= \sqrt{2n_k+1}\sin b_k + \delta_k, \\ p_k^{\text{inital}}(0) &= \sqrt{2n_k+1}\cos b_k, \end{aligned} \tag{7}$$

where the phases b_k are picked randomly from the interval $[0, 2\pi]$, the quantum numbers n_k are sampled according to the Boltzmann distribution $P(n_k) = \exp(-\beta n_k\omega_k)$. $a_k^{-1/2}$ equals the width of the coherent state of a corresponding harmonic oscillator. In Sec. IV of Ref. 14), there was an arbitrary expression for the thermal width

$$a_k = \frac{m_k\omega_k}{\hbar}\left[\coth\left(\frac{\hbar\omega_k}{2k_BT}\right) - \frac{2k_BT}{\hbar\omega_k}\right]^{-1}.$$

We use $q_k^j = q_k^{\text{inital}} - a_k^{-1/2} + j * \Delta q$ and $p_k^j = p_k^{\text{inital}} - \frac{\pi\hbar}{\Delta q} + j * \Delta p$ to sample the initial conditions of the trajectories around the central point q_k and p_k.

C_j is the distribution of initial conditions for the bath trajectory. N_m is the trajectory number, and N is the degree of dimensionality.

$$\begin{aligned} C_j^m &= \prod_{m=1}^{N} w_m(p_m, q_m), \\ w_m(p_m, q_m) &= w_m(p_m) * w_m(q_m), \\ w_m(q_m) &= (2\pi\hbar G_m)^{-1/2} \exp\left[-\frac{1}{2\hbar G_m}(q_m - q_m(0))^2\right] * \Delta q, \\ w_m(p_m) &= (2\hbar G_m/\pi)^{-1/2} \exp[-2\hbar G_m(p_m - p_m(0))^2] * \Delta p. \end{aligned} \tag{8}$$

From Eq. (6) to Eq. (8), we can find that our method is quite different from the conventional semiquantum method. The conventional semiquantum method only

takes into account the central point (q_k,p_k), and does not consider other points (q_k^j,p_k^j). The effect of the points around the central point is ignored. In our method, we not only consider the point (q_k^j,p_k^j), but also consider its own weights. In (6), we introduce the average Gaussian wave packet to represent the wave function. All semiquantal quantities are obtained by evaluating each individual trajectory and averaging them, taking into account their respective probabilities. This is the reason why we call our method the averaged semiquantum method.

Substituting (5) into (4) and using Gaussian integration, we can obtain the averaged semiquantum method working equations. From the interaction Hamiltonian, the associated mean-field dynamics can be obtained according to the variational principle. The influence of the environment on the system only enters through

$$\langle B(t)\rangle_E = -\sum k_n \langle q(t)\rangle. \tag{9}$$

The averaged semiquantum method is obtained by propagating each Gaussian wave packets. This method can track the classical distribution even at times the distribution is highly non-Gaussian and involves quantum coherence in phase space. Furthermore, it contains nontrivial quantum information. In this sense, it is not a semiclassical approximation. The semiquantum energy of system (the first KHO) is

$$\langle E_n(t)\rangle = \sum_{n=0}^{N}\left(\frac{p_{tn}^2}{2m_1}+\frac{1}{2}m_1\omega_0^2 q_{tn}^2+\frac{1}{2}\hbar\left(\frac{1}{4G_{tn}}+4\prod_{tn}^{2}G_{tn}+\omega_0^2 G_{tn}\right)\right)P_t(q_{tn},p_{tn}), \tag{10}$$

where n is the number of the trajectories, and N is the total number of the trajectories. The diffusion is defined by $\langle E_n(t)\rangle$ in which the initial averaging energy $\langle E_0\rangle$ is subtracted.

Except for the variational principle, no approximations are made to obtain equations. Therefore we can study the reduced density matrix from averaging over different paths. We use the decoherence function to measure decoherence of the averaged semiquantum version. Following Refs. 13) and 14), we consider the direct product of the system S and bath B Hilbert spaces. The system space is assumed to be N dimensional. We consider N orthogonal states ϕ_i^S of the system and a system-bath interaction that induces quantum transitions in the combined system, with the bath state responding to that of the system:

$$\begin{aligned}
|\psi\rangle &= |\psi_0\rangle\prod_{k=1}^{N}|\psi_k\rangle \\
&= \left(\sum_i c_i\left|\phi_i^S\right\rangle\right)\left|\phi_0^B\right\rangle \rightarrow \sum_i c_i\left|\phi_i^S\right\rangle\left|\phi_i^B\right\rangle = |\Psi_t\rangle \\
\left|\phi^B\right\rangle &= \sum_{j=1}^{M} C_j\left|\psi_k^j\right\rangle,
\end{aligned} \tag{11}$$

where ϕ_0^B is the initial state of the bath. Transitions from an arbitrary initial system

$\sum_i c_i\phi_i^S$ are then described in terms of the reduced density matrix,

$$\begin{pmatrix} |c_1|^2 & \cdots & c_1c_i^* & \cdots & c_1c_N^* \\ \vdots & \ddots & \vdots & \iddots & \vdots \\ c_ic_1^* & \cdots & |c_i|^2 & \cdots & c_ic_N^* \\ \vdots & \iddots & \vdots & \ddots & \vdots \\ c_Nc_1^* & \cdots & c_Nc_i^* & \cdots & |c_N|^2 \end{pmatrix}$$

$$\rightarrow \begin{pmatrix} |c_1|^2 & \cdots & c_1c_i^*(\phi_i^B\,|\phi_1^B) & \cdots & c_1c_N^*(\phi_N^B\,|\phi_1^B) \\ \vdots & \ddots & \vdots & \iddots & \vdots \\ c_ic_1^*(\phi_1^B\,|\phi_i^B) & \cdots & |c_i|^2 & \cdots & c_ic_N^*(\phi_N^B\,|\phi_i^B) \\ \vdots & \iddots & \vdots & \ddots & \vdots \\ c_Nc_1^*(\phi_1^B\,|\phi_N^B) & \cdots & c_Nc_i^*(\phi_i^B\,|\phi_N^B) & \cdots & |c_N|^2 \end{pmatrix}. \tag{12}$$

Decoherence is defined as decay of the nondiagonal matrix elements, which is clearly determined by the decay of the sum of the inner product of the bath states $\sum_{i\neq j}(\phi_i^B\,|\phi_j^B)$. Within the frozen Gaussian formulation,[15] the decay of the integral and corresponding nondiagonal matrix elements is described by the decoherence function given by Eq. (39) of Ref. 16). The decoherence function in the frozen Gaussian approximation is completely determined by the real valued nuclear overlap integral.

$$\begin{aligned} D(t) &= 1 - \sum_{i\neq j} \left| c_jc_i^*(\phi_i^B\,|\phi_j^B)\right| \approx 1 - \sum_{i\neq j} |\,c_jc_i^*J_{\text{overlap}}(t)| \\ &= 1 - \sum_{i\neq j} c_jc_i^* \prod_n \exp(-0.25(\bar{q}_{jn}(t) - \bar{q}_{in}(t))^2/\bar{G}_n) \\ &\quad \times \exp(-0.25 * \bar{G}_{n(}(\bar{p}_{jn}(t) - \bar{p}_{in}(t))^2/\hbar^2) \\ &\quad \times \cos(-0.5(\bar{q}_{jn}(t) - \bar{q}_{in}(t))(\bar{p}_{jn}(t) + \bar{p}_{in}(t))/\hbar), \end{aligned} \tag{13}$$

where $\bar{h}$ denotes the statistic average time-dependent physical quantity h along its trajectory in phase space. Using these, we can study decoherence.

§3. Low dimensional KHO model

We use the split operator scheme[17] to investigate how the quantum interference is eliminated by noise[18] and whether the averaged semiquantum method can predict quantum-classical correspondence by comparing the diffusions of the harmonic oscillator for one-dimensional quantum KHO. For the two coupled quantum KHO, we use Chebyshev scheme to perform the numerical calculations in the eigenrepresentation of two harmonic oscillators.[19),20] The Chebyshev scheme can give us high precise results for a long time.

The Hamiltonian of one-dimensional KHO reads

$$H = \frac{p^2}{2m} + \frac{1}{2}m\omega_0^2q^2 - K\cos(q)\sum_{n=0}^{\infty}\delta(t-n\tau) + \lambda\Delta_n\sin(q+\alpha_n)\sum_{n=0}^{\infty}\delta(t-n\tau), \tag{14}$$

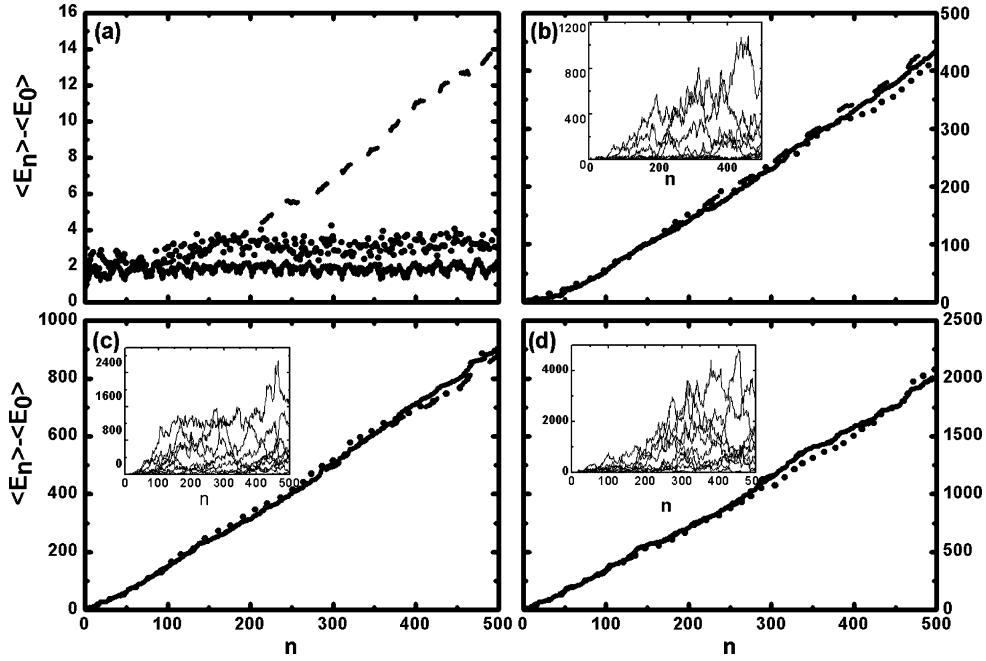

Fig. 1. Quantum (solid), semiquantum (dot) and classical (dash) diffusion vs time (kick number) for one-dimensional KHO by adding noise with $\tau = 0.4\pi, \hbar = 1$, and $K = 2$. From (a) to (d), $\lambda = 0.0$, 2.0, 5.0, and 10.0. Inset: mean energy of one Gaussian wave packet, starting from different (q_0, p_0).

where Δ_n is a Gaussian random variable, and α_n is random with uniform distribution in $[0, 2\pi]$.

There is dynamical localization[24] for quantum KHO for the condition $K = 2$, $\tau = 0.4\pi$, $\lambda = 0$. The quantum diffusion is suppressed by the quantum interference. As shown in Fig. 1(a), both quantum and semiquantum behavior are localized, while the classical energy increases. This results in the breakdown of the classical-quantum correspondence. As λ increases, the noise makes the delocalization of quantum and semiquantum KHO. Figure 1(b) shows that there is a small difference among the diffusion of quantum, semiquantum, and classical KHO. The difference is almost invisible for larger λ, as shown in Fig. 1(c) and Fig. 1(d) respectively. It is because that the increase of λ can induce enough noise to destroy the quantum localization, eliminate the quantum interference and produce quantum-classical correspondence. Furthermore, the averaged semiquantum method can predict quantum-classical correspondence well. When the classical-quantum diffusion is not correspondence, semiquantum diffusion is between them. When the difference of diffusion is almost invisible, semiquantum version produces the similar results.

To confirm that the averaged semiquantum method can predict decoherence, we show the diffusions of the two coupled quantum KHO with discontinuous potential. Comparing with one dimension case, we find the second KHO plays a similar role as the noise. λ is the coupling strength, acting as the second kick $\lambda\Delta_n$. Like α_n, q_2 can also induce random numbers with uniform distribution in $[0, 2\pi]$, because of the

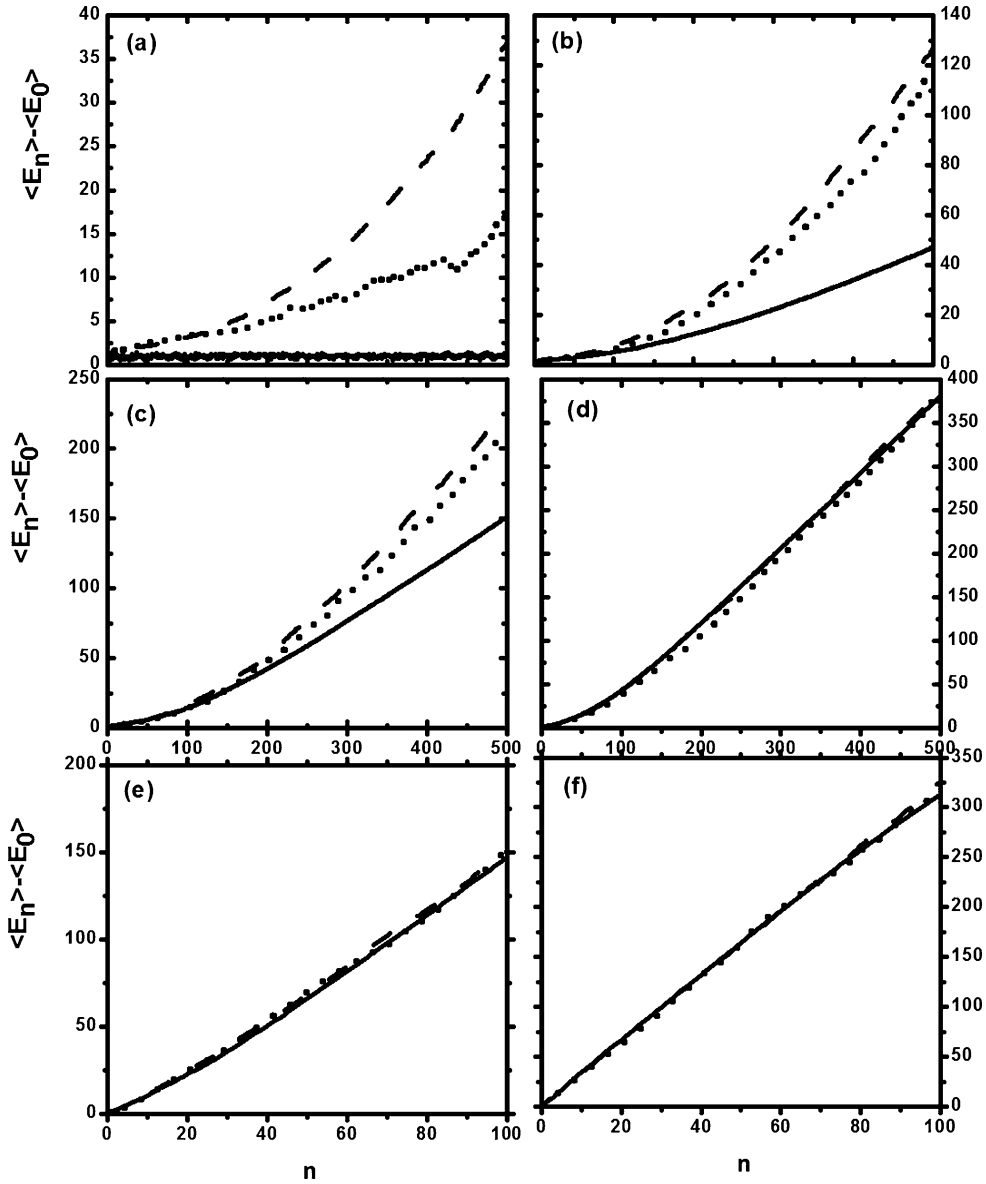

Fig. 2. Quantum (solid), semiquantum (dot), and classical (dash) diffusion vs time for two coupled KHO with discontinuous potential with $\tau = 0.4\pi, \hbar = 1$, and $K = 2$. From (a) to (f), $\lambda = 0.1$, 0.3, 0.5, 0.8, 1.6, and 3.0.

periodicity of sin function.

For $\lambda < 0.8$, the quantum version increases slower than the classical counterpart, while the semiquantum one is between them as shown in Figs. 2(a)–(c). As the coupling strength increases, the differences among the quantum, the semiquantum and the classical energy decrease. For $\lambda \geq 0.8$, there is almost no difference between the quantum diffusion and the classical one. When the difference energy between the

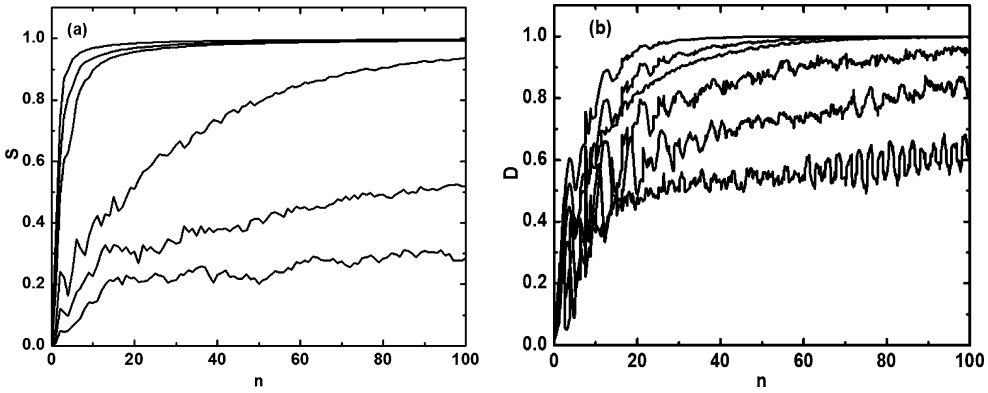

Fig. 3. From bottom to top, λ= 0.3, 0.5, 0.8, 1.6, 2.0, and 3.0. (a) Linear entropy vs time. (b) Decoherence function vs time.

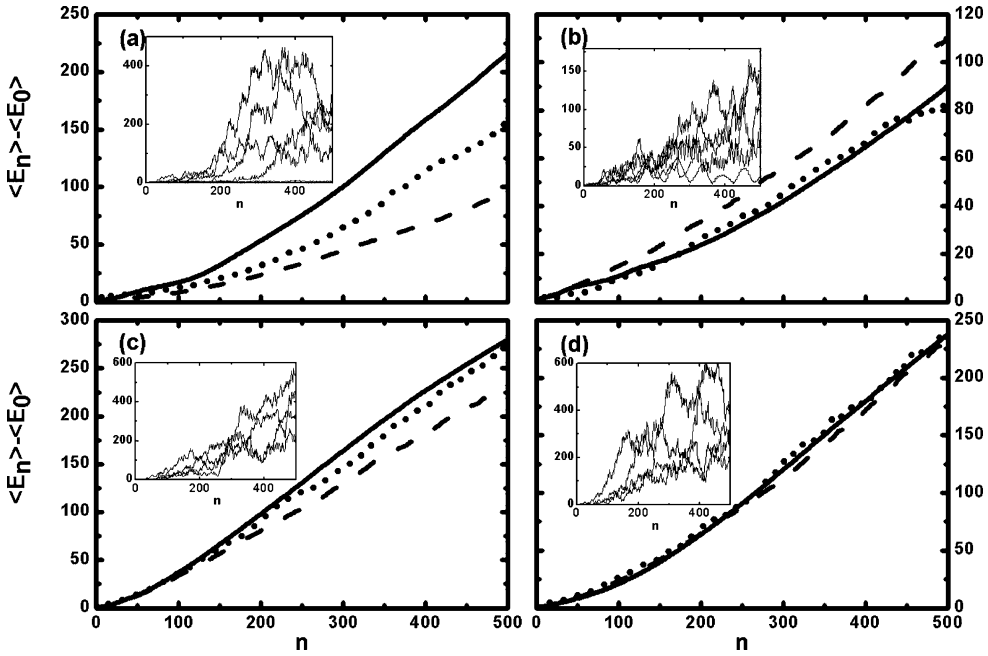

Fig. 4. Quantum (solid), semiquantum (dot), and classical (dash) diffusion vs time for two coupled KHO with continuous potential. $\tau = 0.4\pi, \hbar = 1$, and $K = 2$. From (a) to (d), $\lambda = 0.2$, 0.3, 0.8, 0.9. Inset: mean energy of one Gaussian wave packet, starting from different $(q_0, p_0; q_1, p_1)$.

classical and quantum disappears, the diffusion of the semiquantum energy agrees fairly well with them. Comparing with one dimension case, we find that q_2 plays a similar role as α_n. Although α_n is completely stochastic and q_2 is governed by the dynamical equation, both α_n and q_2 can produce enough noise to eliminate the quantum interferences for strong coupling strength.

Furthermore, we want to study whether the decoherence function can predict decoherence in two-dimensional KHO. We use the linear entropy S, which is defined

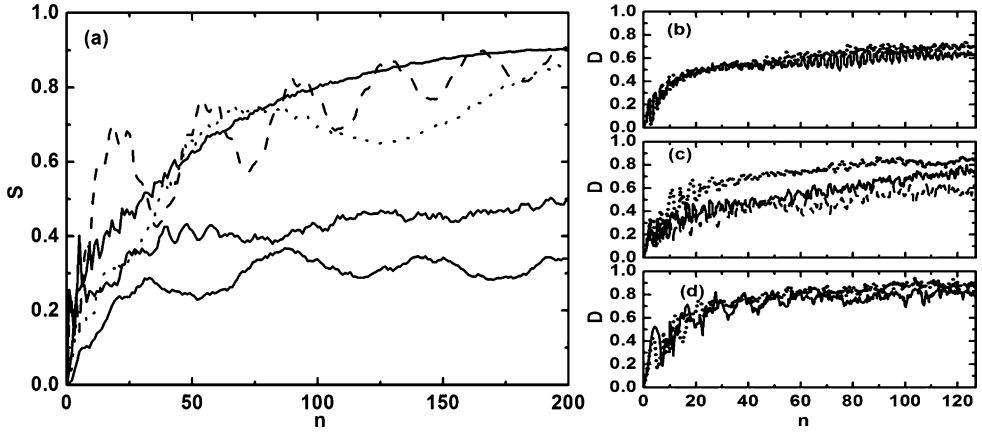

Fig. 5. Two coupled KHO with continuous potential for $\tau = 0.4\pi, \hbar = 1$, and $K = 2$. (a) Linear entropy vs time. From bottom to top, $\lambda = 0.1$, 0.3, 0.2 (dot), 0.8 (dash), and 0.9. (b) Decoherence function vs time $\lambda = 0.2$ (dot), 0.3. (c) $\lambda = 0.5$, 0.6 (dash), 0.7 (dot). (d) $\lambda = 0.8$ (dot), and 0.9.

by $S = 1 - \mathrm{tr}(\rho_A^2)$ with $\rho_A = \mathrm{tr}_B(\rho_{AB})$,$\rho_{AB} = |\psi_{AB}\rangle \langle\psi_{AB}|$, to measure the quantum decoherence. As shown in Fig. 3(a), both the production rate of S and the saturation values increase as increasing λ. Comparing the result of entropy with the decoherence function shown in Fig. 3(b), we find that the production rate of decoherence function has the similar increase, although the saturation values are different for small λ. When $\lambda \geq 0.8$, the saturation values are similar to the linear entropy. The decoherence function predicts the decoherence well.

The result for the two coupled KHO with continuous potential is shown in Fig. 4. We also find that the difference among the quantum, semiquantum, and classical diffusion decreases with the increase of the coupling strength. However, It is somewhat surprising that the quantum diffusion is larger than the corresponding classical one, shown in Figs. 4(a) and (c). Accordingly, the linear entropy increases more quickly when $\lambda = 0.2$ (dotted line) than when $\lambda = 0.3$ in Fig. 5(a). Similarly, Fig. 5(b) also displays that the increase of decoherence function is faster when $\lambda = 0.2$ (dotted line) than when $\lambda = 0.3$. In Fig. 5(d), we find that $D(\lambda = 0.8)$ is close to $\lambda = 0.9$ which can be also found in Fig. 5(a). The phenomenon, which is not found for discontinuous coupling potential, is caused by the continuous coupling potential. If S increases rapidly, the effects of decoupling and decoherence are intense. This leads to the diffusion of the wave packet and the increase of the quantum energy. The rapid linear entropy growth results in the quantum energy diffuse quickly. Comparing the result of entropy with the decoherence function, it shows that the decoherence function can predict the decoherence well.

From the above results, we see that the semiquantum method can mimic many true quantum behaviors, though it is a kind of approximation. The calculation of the quantum version is very time-consuming for two or high dimensional KHO, but the averaged semiquantum method is more efficient. This indicates that the averaged semiquantum method is a useful tool to predict the decoherence and to

find the quantum-classical correspondence. Semiquantal diffusions of one Gaussian wave packet are obtained by evaluating individual trajectory shown in the inset of Figs. 1 and 3, starting from different (q_i, p_i). Because of the quantum fluctuations, the results cannot predict the quantum-classical correspondence well. However, the evolving of an ensemble of trajectories can give much better results, as it can reduce the statistical dispersion and improve the numerical accuracy.

§4. Comparison with the result of master equation

To confirm that the averaged semiquantum method can predict decoherence, following Refs. 21) and 22), we illustrate numerically the decoherence of a superposition of two symmetrically located coherent states, which have been intensively investigated by master equation. The Hamiltonian of this system is Eq. (1) without kick terms, and the environment is a heat bath of oscillators. Our aim is to illustrate various decoherence scenarios for quantum superposition $|\varphi\rangle = c_1 |\varphi_1\rangle + c_2 |\varphi_2\rangle$ by using averaged semiquantum method. In Refs. 21) and 22), the authors employ the norm $N_{12}(t) = \mathrm{Tr}_{\mathrm{sys}}\rho^{12}_{\mathrm{sys}}(t)\rho^{21}_{\mathrm{sys}}(t)^{+}$ as an indicator of the temporal fate of the relative coherence between the two superposed wave packets. Clearly, if the system were closed, its unitary time evolution would leave that norm constant in time ($N_{12}(t) = 1$); interaction with a many-freedom environment will cause decay. The dynamics of the system is determined by the reduced density operator$\rho_{\mathrm{sys}}(t) \equiv \rho_t$. Assuming initial decorrelation of system and bath, we encounter the following well-known evolution equation:

$$\dot{\rho}_t = \frac{1}{i\hbar}[H_{\mathrm{sys}}, \rho_t] + \frac{a_t}{2i\hbar}[q^2, \rho_t] + \frac{b_t}{2i\hbar}[q, \{p, \rho_t\}] + \frac{c_t}{\hbar^2}[q, [p, \rho_t]] - \frac{d_t}{\hbar^2}[q, [q, \rho_t]], \quad (15)$$

where a_t, b_t mean the drift coefficient, and c_t, d_t the diffusion coefficients. In terms of the Wigner function, Eq. (15) takes the form of a Fokker-Planck equation

$$\dot{W}_t = \left(-\frac{\partial}{\partial q}\frac{p}{M} + \frac{\partial}{\partial p}\{(M\Omega^2 + a_t)q + b_t p\} + c_t\frac{\partial^2}{\partial p \partial q} + d_t\frac{\partial^2}{\partial p^2} \right) W_t. \quad (16)$$

We can solve Eq. (16) with the help of the Fourier transform of the Wigner function, and diffusive effects on W can be confined to a Gaussian factor in χ.

$$\chi_t(\mu, v) = \zeta_t(\mu, v) \exp\left(\int_0^t b(s)ds \right) \exp\left(-\frac{1}{2\hbar}\{\alpha_t\mu^2 + 2\beta_t\mu v + \gamma_t v^2\} \right). \quad (17)$$

The cofactor ζ obeys the Liouville equation and provides the time-dependent coefficients α, β, γ in Eq. (17) that satisfy the linear equations

$$\begin{pmatrix} \dot{\alpha}_t \\ \dot{\beta}_t \\ \dot{\gamma}_t \end{pmatrix} = \begin{pmatrix} 0 & -2/M & 0 \\ M\Omega^2 + a_t & -b_t & -1/M \\ 0 & 2(M\Omega^2 + a_t) & -2b_t \end{pmatrix} \begin{pmatrix} \alpha_t \\ \beta_t \\ \gamma_t \end{pmatrix} + \begin{pmatrix} 0 \\ -c_t \\ 2d_t \end{pmatrix}. \quad (18)$$

In the Golden rule limiting cases, we replace the 3×3 propagator matrix in the evolution equation (18) in zeroth order by entirely neglecting a_t and b_t, and replace

the time-dependent coefficients of the exact master equation (15) by the lowest-order expressions. In the interaction dominance, we expand all dynamical quantities connected to the oscillator dynamics to the lowest relevant order in t.

Similarly to the $N_{12}(t)$, we employ the norm $n_{12}(t) = \mathrm{Tr}_{\mathrm{sys}}\rho^{12}_{\mathrm{sys}}(t)\rho^{21}_{\mathrm{sys}}(t)^{+}$ to measure the relative coherence between the two superposed wave packets. If the system interacts with a many-freedom environment,

$$\begin{aligned} n_{12}(t) &= \left\langle \bar{\phi}^B_2(t) \mid \bar{\phi}^B_1(t) \right\rangle \left\langle \bar{\phi}^B_1(t) \mid \bar{\phi}^B_2(t) \right\rangle \\ &= \prod_n \exp(-0.5(\bar{q}_{1n}(t) - \bar{q}_{2n}(t))^2/\bar{G}_n - 0.5\bar{G}_n(\bar{p}_{1n}(t) - \bar{p}_{2n}(t))^2/\hbar^2). \quad (19) \end{aligned}$$

We choose that the cutoff frequency equals 100 Ω and $\omega_i \in [1, 100]$ obtained from uniform random number, and approximate the thermal energy by sampling from a classical canonical distribution and let the thermal energy equal $20\hbar\Omega$. Furthermore, we compare our results obtained by semiquantum method with the results from master equation.

In Figs. 6(a)–(c), we show the decay of n_{12} of initial superposition with different separation (d_Q). The dashed and dash-dotted lines represent the golden-rule result and interaction-dominance result. The solid lines represent the semiquantum numerical results with different dimensionality. When $d_Q = 16$, the saturated value of n_{12} is about 0.88 at $N = 20$. The decay of n_{12} changes from saturated to linear at $N = 36$, and from linear to exponential with the increase of the dimensionality $N = 70$, which is close to the golden-rule results. When $N \geq 80$, the trend of the decay is almost changeless. In Figs. 6(c) and (d), we also show the decay of n_{12} with separation $d_Q = 80$ and $d_Q = 4000$ with different dimensionality, and find that the n_{12} decrease more quickly with the increase of N. The decays of n_{12} are almost unchanged for $N \geq 70$ and $N \geq 30$ respectively. The critical value of N decreases with the increase of the d_Q, when the decay reaches a plateau. Furthermore, we also find the various decoherence scenarios: golden-rule, crossover, and interaction-dominated regime. At $d_Q = 16$ and $N = 80$, the semiquantum result is close to the golden-rule. When $d_Q = 80$ and $N \geq 70$, the results are between the golden-rule line and interaction-dominance line. For $d_Q = 4000$ and $N \geq 30$, the full line fits the interaction-dominance line well. These results not only agree with the ones obtained by master equation method, but also show how the dimensionality of the external system affects the relative coherence between the two superposed wave packets.

§5. High dimensional case

In this section, we want to show the classical-semiquantum transition and decoherence for high dimensional KHO. For $N = 30$ and $\lambda = 0.05$ shown in Fig. 7(a), the classical energy is completely different from the quantum one. With the increase of λ, Fig. 7(b) shows that the semiquantum diffusion is close to the classical one. And the larger λ leads to the semiquantum-classical correspondence shown in Figs. 7(c) and (d). From the inset figures of Fig. 7, we find the similar phenomena of the semiquantum-classical transition. Moreover, we can find the semiquantum-classical correspondence for a smaller λ when N is larger. The inset figure of Fig. 7(a),

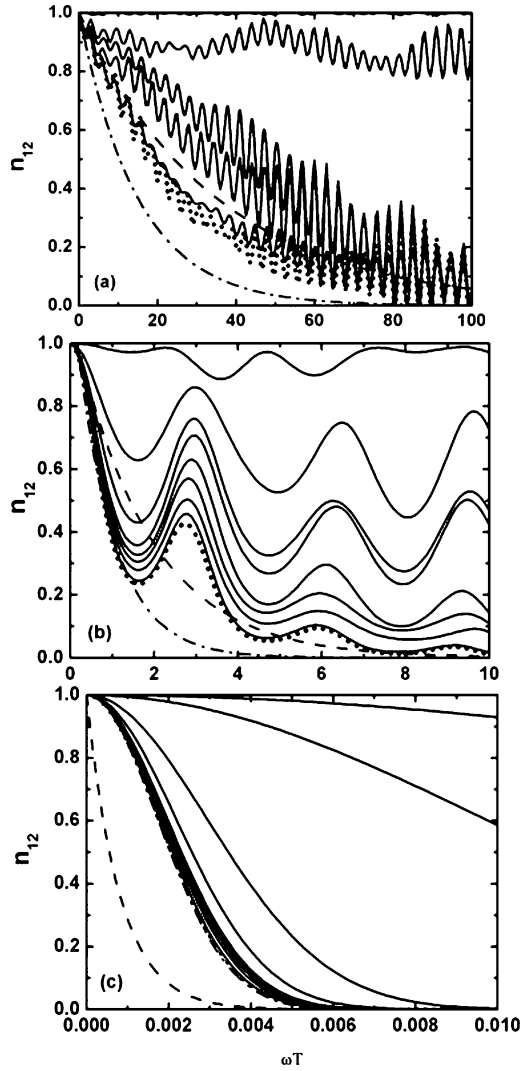

Fig. 6. n_{12} vs time. Dashed lines: golden-rule result. Dash-dotted lines: interaction-dominance results. Solid lines: Semiquantum results. From top to bottom, (a) $N = 20$, 36, 50, 70, 80 (dot). $d_Q = 16$. (b) $N = 5$, 10, 20, 30, 40, 50, 60, 70, 80 (dot). $d_Q = 80$. (c) $N = 2$, 5, 10, 20, 30, 50, 60, 70, 80 (dot). $d_Q = 4000$.

at $\lambda = 0.1$, displays the better semiquantum-classical correspondence than the one at $N = 30, \lambda = 0.2$. When $N = 60, \lambda = 0.1$, we can find the improve agreement of the semiquantum and classical versions. We also find the semiquantum-classical correspondence at $\lambda = 0.05$ for larger N ($N = 80$). It means that both the stronger coupling strength and the larger dimensionality of the bath can lead to the faster classical-quantum correspondence. Semiquantal diffusions of one Gaussian wave packet obtained by evaluating individual trajectory are shown in the inset figures of Fig. 7(d).

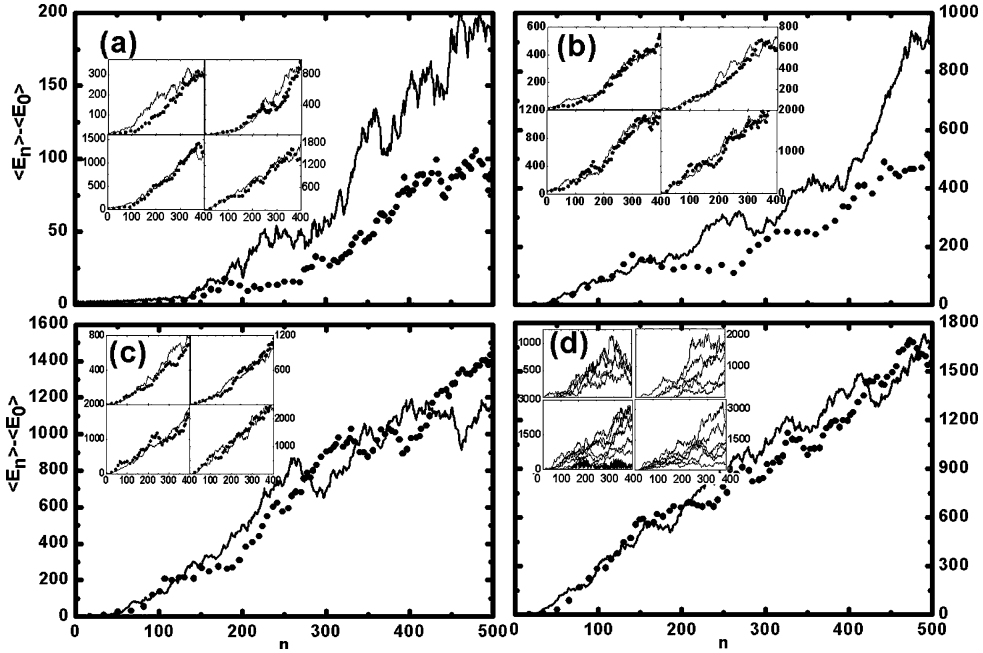

Fig. 7. Semiquantum (dot), and classical (dash) mean energy vs time for $\tau = 0.4\pi, \hbar = 1, N = 30$ and $K = 2$. From (a) to (d), $\lambda = 0.05$, 0.1, 0.2, and 0.3. Inset (a): $N = 40$, $\lambda = 0.05$, 0.1, 0.2, and 0.3. Inset (b): $N = 60$, $\lambda = 0.05$, 0.1, 0.2, and 0.3. Inset (c): $N = 80$, $\lambda = 0.05$, 0.1, 0.2, and 0.3. Inset (d): mean energy of one Gaussian wave packet, starting from different $(q_0, p_0; \ldots; q_i, p_i)$. $N = 30$, $\lambda = 0.05$, 0.1, 0.2.

To measure the decoherence, we calculate the decoherence function of the coupled KHO model with different dimensionalities and coupling strength. $1 - D$ describes the sum of nondiagonal matrix elements, the behaviors of which are shown in Fig. 8. Three different $1 - D$ decreases have been observed, namely decrease to saturate value (decreases to some saturate value), linear decrease, and exponential decrease. For the small λ and N, we find the rate of $1 - D$ decreases linearly down to some saturate value (not zero). This means that the nondiagonal matrix elements have not reduced to zero yet. Furthermore, the saturated value reduces with the growth λ for the same dimensionality. Similarly, the larger the dimensionality is, the smaller the saturated value is for the same λ. The decay of $1 - D$ changes from saturate to linear decrease with suitable λ and N, by comparing short dashed line and short dotted line shown in Figs. 8(a) and (b). When $N = 25, 35, \lambda = 0.1$ and $N = 20, \lambda = 0.2$, the decoherence functions decrease linearly to zero with different slopes, shown in Figs. 8(b) and (c), because the sum of the nondiagonal matrix elements decreases to zero. For the higher bath's dimensionality and the stronger coupling strength, a respective comparison of short dashed line and short dotted line in Fig. 8 with short dashed line and short dotted line in Fig. 9 shows the manner of decrease changes from linearity to exponent decrease. And the decrease of exponent manner is faster than the linearity manner. When $N \geq 40$, the tendency of the decoherence function is almost unchanged.

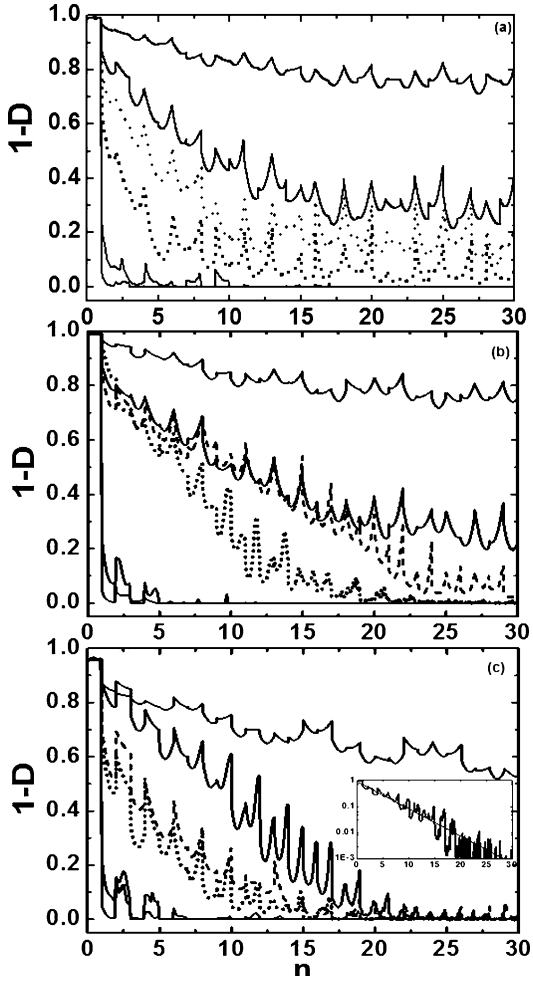

Fig. 8. $1 - D$ vs time. From top to bottom, $N = 10$, 20, 25 (short dash), 35 (short dot), 40, 80. (a) $\lambda = 0.05$, (b) $\lambda = 0.1$, (c) $\lambda = 0.2$. Inset: $N = 25$, asymptotic line $D = 0.9 * \exp(-0.24 * n)$.

§6. Conclusion

For the model of coupled KHO, we show that the semiquantum method is able to predict decoherence. Decoherence function is used to measure the decoherence. The larger the dimensionalities and coupling strengths are, the faster the corresponding decoherence is. The manner of decoherence function changes from saturated, linear to exponential function, with the increase of the dimensionality and coupling strength. For $N \geq 40$, the transformations of the decoherence function are almost unchanged. Furthermore, the averaged semiquantum method agrees with the prediction of master equation. These indicate that semiquantum method is useful to study the quantum-classical correspondence in the high dimensionality system.

References

1) W. V. Liu and W. C. Schieve, Phys. Rev. Lett. **78** (1997), 3278.
   A. K. Pattanayak and W. C. Schieve, Phys. Rev. E **56** (1997), 278.
2) B. Hu, B. Li, J. Liu and J. L. Zhou, Phys. Rev. E **58** (1998), 1743.
3) A. K. Pattanayak and W. C. Schieve, Phys. Rev. E **50** (1994), 3601.
4) R. Jackiw and A. Kerman, Phys. Lett. A **71** (1979), 158.
5) Y. Tsue and Y. Fujiwara, Prog. Theor. Phys. **86** (1991), 433.
6) B. Hu and B. Li, Physica A **288** (2000), 81.
7) M. A. de Ponte, M. C. de Oliveira and M. H. Y. Moussa, Phys. Rev. A **70** (2004), 022324.
   M. A. de Ponte, S. S. Mizrahi and M. H. Y. Moussa, Phys. Rev. A **76** (2007), 032101.
8) G. M. Zaslavsky et al., Zh. Eksp. Teor. Fiz. **91** (1986), 500.
   A. A. Chernikov et al., Physica D **33** (1988), 65.
   A. J. Lichtenberg and B. P. Wood, Phys. Rev. A **39** (1989), 2153.
   I. Dana and M. Amit, Phys. Rev. E. **51** (1995), R2731, and references therein.
9) B. Hu, B. Li, J.Liu and Y. Gu, Phys. Rev. Lett. **82** (1999), 4224.
10) R. Sankaranarayanan, A. Lakshminarayan and V. B. Sheorey, Phys. Rev. E. **64** (2001), 046210.
11) F. Borgonovi and L. Rebuzzini, Phys. Rev. E **52** (1995), 2302.
12) G. A. Kells, J. Twamley and D. M. Heffernan, Phys. Rev. E **70** (2004), 015203.
13) W. H. Zurek, Rev. Mod. Phys. **75** (2003), 715.
14) O. V. Prezhdo and P. J. Rossky, Phys. Rev. Lett. **81** (1998), 5294.
15) E. J. Heller, J. Chem. Phys. **75** (1981), 2923.
16) O. V. Prezhdo and P. J. Rossky, J. Chem. Phys. **107** (1997), 5863.
17) C. Leforestier et al., J. Comput. Phys. **94** (1991), 59.
18) E. Ott, T. M. Antonsen and J. D. Hanson, Phys. Rev. Lett. **53** (1984), 2187.
19) G. P. Berman et al., Nonlinearity **4** (1991), 543.
20) G. T. Vega, J. Chem. Phys. **99** (1993), 1824.
21) W. T. Strunz and F. Haake, Phys. Rev. A **67** (2003), 022101.
22) W. T. Strunz and F. Haake, Phys. Rev. A **67** (2003), 022102.
23) T. Dittrich and R. Graham, Ann. of Phys. **200** (1990), 363.
24) P. W. O'Connor and E. J. Heller, Phys. Rev. Lett. **61** (1988), 2288.
   E. J. Heller, Phys. Rev. A **35** (1987), 1360.
   F. Borgonovi, G. Casati and B. Li, Phys. Rev. Lett. **77** (1996), 4744.
   A. Schmid, Phys. Rev. Lett. **51** (1983), 1506.
   S. Yoshida, F. Großmann, E. Persson and J. Burgdörfer, Phys. Rev. A **69** (2004), 043410.